

# An Integrative Genome-Scale Metabolic Modeling and Machine Learning Framework for Predicting and Optimizing Biofuel-Relevant Biomass Production in *Saccharomyces cerevisiae*

Neha K. Nair

Department of Physics and Chemistry  
National Institute of Technology, Warangal  
Warangal, India

nk23edi0017@student.nitw.ac.in

Aaron D'Souza

Department of Electronics and Communication Engineering  
National Institute of Technology, Warangal  
Warangal, India

ad22ecb0f20@student.nitw.ac.in

**Abstract**—*Saccharomyces cerevisiae* is a cornerstone organism in industrial biotechnology and metabolic engineering, owing to its genetic tractability, well-characterised metabolism, and robust fermentative capacity. Despite decades of study, accurately predicting biomass flux across diverse environmental and genetic perturbations remains a significant challenge, limiting the rational design of strains for biofuel production. This study presents a comprehensive computational framework that combines the Yeast9 genome-scale metabolic model (GEM) with machine learning (ML) and optimisation techniques to systematically predict, interpret, and enhance biomass flux in yeast. Flux balance analysis (FBA) was used to generate a detailed dataset of metabolic flux distributions by varying glucose, oxygen, and ammonium uptake rates. These simulated profiles trained Random Forest and XGBoost regressors, which achieved coefficients of determination ( $R^2$ ) of 0.99989 and 0.9990, respectively. A feed-forward neural network (FFNN) captured nonlinear flux-biomass relationships, while a variational autoencoder (VAE) uncovered four distinct metabolic clusters in latent space. SHAP-based feature attribution identified the top twenty most influential reactions, implicating glycolysis, the TCA cycle, and lipid biosynthesis as key contributors to biomass yield. *In silico* overexpression of key reactions achieved a biomass flux of 0.979 gDW·hr<sup>-1</sup>. Bayesian optimisation of nutrient uptake constraints produced a 12-fold increase in predicted biomass flux (from 0.0858 to 1.041 gDW·hr<sup>-1</sup>). A generative adversarial network (GAN) proposed novel metabolic flux configurations consistent with stoichiometric feasibility, yielding a generated variance of 0.156. This framework demonstrates how GEM-based simulation, interpretable ML, and generative modelling can significantly advance the understanding and manipulation of yeast metabolism. Further experimental validation is required to confirm the predicted metabolic improvements.

**Index Terms**—*Saccharomyces cerevisiae*, genome-scale metabolic model, flux balance analysis, SHAP, Bayesian optimisation, biofuel, machine learning, generative adversarial network

## I. INTRODUCTION

*Saccharomyces cerevisiae* plays a vital role in fundamental cell biology and applied industrial biotechnology. Its well-annotated genome, tolerance to inhibitory fermentation conditions, and capacity to produce ethanol and other biofuel

products make it an organism of enduring interest for sustainable energy applications [1]. The rational engineering of yeast strains toward maximised biomass or product yields is complicated by the extraordinary complexity of eukaryotic metabolism: thousands of enzymatic reactions, tightly regulated gene expression programmes, and condition-dependent flux rerouting collectively confound straightforward prediction of cellular behaviour from first principles.

Genome-scale metabolic models (GEMs) address this complexity by encoding the full stoichiometric network of metabolic reactions and providing a computational substrate for constraint-based analyses such as flux balance analysis (FBA) [4]. The Yeast9 consensus GEM [2] comprises 4,131 reactions, 2,806 metabolites, and 1,161 genes, making it one of the most comprehensive metabolic models available for any eukaryote [5]. FBA identifies optimal flux distributions consistent with stoichiometric, thermodynamic, and capacity constraints, enabling rapid *in silico* screening of genetic and environmental perturbations.

Machine learning provides a powerful complement to constraint-based metabolic modelling. Supervised models such as Random Forest and XGBoost extract predictive relationships from high-dimensional flux datasets, while deep learning architectures enable nonlinear pattern recognition and unsupervised representation learning [6], [7], [11]. SHAP (SHapley Additive exPlanations) values provide a model-agnostic approach to feature attribution, enabling the identification of specific reactions whose flux variation most strongly influences predicted biomass [10]. Generative models such as GANs can synthesise novel flux configurations for *de novo* metabolic pathway discovery [18], [20], [25].

Despite the growing body of literature at the intersection of GEMs and ML, most studies address narrow objectives without providing a unified, end-to-end pipeline that encompasses data generation, prediction, interpretation, and optimisation [7], [8]. This fragmentation limits reproducibility and the translation of computational findings into experimental

hypotheses.

The present study addresses this gap by developing an integrative computational pipeline for *S. cerevisiae* that encompasses: (i) GEM-based FBA data generation across systematically varied environmental conditions; (ii) dimensionality reduction and unsupervised clustering via VAE and K-means; (iii) supervised biomass flux prediction using Random Forest, XGBoost, and FFNN; (iv) reaction-level interpretation via SHAP analysis; (v) *in silico* overexpression and knockout perturbation studies; (vi) oxygen sensitivity analysis; (vii) Bayesian optimisation of nutrient uptake parameters; and (viii) GAN-based generation of novel metabolic flux profiles.

## II. RELATED WORK

### A. Genome-Scale Metabolic Modelling of Yeast

The Yeast8 consensus GEM provided a comprehensively annotated metabolic network supporting diverse constraint-based analyses [1]. The subsequent Yeast9 model introduced thermodynamic feasibility constraints, enabling more physiologically grounded flux predictions and expanding pathway coverage [2]. GEM-based studies have been applied across a wide spectrum of phenotypic objectives, including ethanol yield optimisation, lipid accumulation for biodiesel production, growth under nutrient limitation, and stress response characterisation [5]. The COBRApy toolbox [3] provides a flexible Python interface for these analyses, facilitating reproducible and programmable metabolic simulations.

Despite their utility, FBA solutions are not unique: many flux distributions can achieve the same objective value, and the deterministic, steady-state assumption underlying FBA does not capture dynamic regulatory responses or stochastic gene expression [8]. These limitations motivate the integration of statistical and machine learning methods that can learn from ensembles of GEM-simulated conditions.

### B. Machine Learning for Metabolic Prediction

The integration of ML with metabolic modelling has gained momentum as the volume and dimensionality of omics data have grown. Ensemble methods such as Random Forest and XGBoost have demonstrated strong performance in predicting growth rates and product yields from flux or omics features [11]. Variational autoencoders (VAEs) have been employed to learn compressed, biologically meaningful latent representations of metabolic flux space [15], [17]. Feed-forward neural networks trained on GEM-simulated data have shown capacity to generalise predictions to unseen environmental conditions [9], [19].

SHAP-based interpretability methods have been applied to biological models to identify which molecular features most influence predicted outcomes [10]. Bayesian optimisation has emerged as an efficient strategy for navigating high-dimensional parameter spaces in metabolic engineering [12], [13]. GANs are increasingly explored for the generation of novel biological sequences, metabolic flux configurations, and synthetic pathway designs [18], [20].

### C. Research Gap and Motivation

Prior integrative studies have generally addressed isolated components of the modelling pipeline without delivering a cohesive, end-to-end framework connecting simulation, prediction, interpretation, and optimisation [7], [8]. Furthermore, few studies have incorporated generative modelling for novel pathway synthesis within a GEM-constrained setting [20], [25]. The present work addresses these limitations by providing a unified pipeline applicable to *S. cerevisiae* and extensible to other industrially relevant microorganisms.

## III. METHODOLOGY

This study integrates genome-scale metabolic modelling with machine learning, deep learning, and optimisation techniques to predict and maximise biomass flux in *Saccharomyces cerevisiae*. The workflow comprises four principal stages: (i) GEM-based flux simulation, (ii) dimensionality reduction and metabolic state clustering, (iii) supervised predictive modelling with feature attribution, and (iv) generative modelling and environmental optimisation. All simulations and model training were implemented in Python using COBRApy [3], scikit-learn, XGBoost, PyTorch, and GPyOpt. All experiments were conducted with fixed random seeds to ensure reproducibility.

### A. Genome-Scale Metabolic Model Simulations

The Yeast9 consensus GEM, comprising 4,131 reactions, 2,806 metabolites, and 1,161 genes, was used as the metabolic network substrate. The biomass objective reaction is  $r_{2111}$ . FBA was applied to compute steady-state flux distributions maximising the biomass objective reaction under systematically varied environmental constraints. Glucose uptake bounds were set at  $(-1.0, 1000.0)$   $\text{mmol}\cdot\text{gDW}^{-1}\cdot\text{hr}^{-1}$  under default conditions, while oxygen uptake bounds were  $(-1000.0, 1000.0)$   $\text{mmol}\cdot\text{gDW}^{-1}\cdot\text{hr}^{-1}$ . These constraints were systematically varied across physiologically relevant ranges, generating a dataset of 2,000 flux profiles each of dimension 4,131, capturing the metabolic response of yeast to a broad range of nutrient availabilities.

### B. Dimensionality Reduction and Unsupervised Clustering

A variational autoencoder (VAE) was trained on the high-dimensional flux dataset to learn a low-dimensional latent representation preserving the principal sources of metabolic variation. The encoder maps each flux vector to a probabilistic latent distribution parameterised by mean and log-variance; the decoder reconstructs the original flux profile from samples drawn from this distribution. The training objective combines a reconstruction loss with a Kullback–Leibler (KL) divergence term that regularises the latent space toward a standard normal prior.

PCA was applied to the two-dimensional latent embeddings to facilitate visualisation and to estimate the optimal number of clusters via the elbow method and silhouette scoring. K-means clustering partitioned the dataset into four metabolic clusters (labels 0–3), corresponding to distinct biomass productivity regimes.

### C. Supervised Predictive Modelling

Three supervised regression models were trained to predict biomass flux from the 4,131-dimensional flux feature vectors. The dataset was split into training (70%), validation (15%), and test (15%) sets. Hyperparameter tuning was performed exclusively on the validation set; the test set was strictly held out for final performance evaluation. Five-fold cross-validation was conducted on the training set.

**Random Forest Regressor:** An ensemble of decision trees trained with hyperparameters selected by grid-search cross-validation. A test  $R^2$  of 0.99989 was obtained, and a 5-fold CV mean  $R^2$  of  $0.99991 \pm 0.00005$  was achieved.

**XGBoost Regressor:** A gradient-boosted tree ensemble with regularisation parameters tuned to balance bias and variance, achieving a test  $R^2$  of 0.9990.

**Feed-Forward Neural Network (FFNN):** A multilayer perceptron with ReLU activations and dropout regularisation trained using the Adam optimiser. Hyperparameters—including hidden layer dimensions, learning rate, and dropout rate—were optimised via grid search to capture higher-order nonlinear flux–biomass relationships.

Model performance was assessed using  $R^2$  and mean squared error (MSE). Statistical consistency was evaluated via standard deviation across cross-validation folds.

### D. Feature Attribution via SHAP Analysis

SHAP (SHapley Additive exPlanations) values were computed for the trained Random Forest model [10] to identify the metabolic reactions most critically governing biomass yield. SHAP values decompose individual predictions into additive contributions from each feature, providing both global importance rankings and local, sample-specific explanations grounded in cooperative game theory [8], [10]. The twenty highest-ranked reactions by mean absolute SHAP value were selected for downstream interpretation and *in silico* perturbation. Results were visualised using beeswarm plots and cluster-stratified heatmaps.

### E. In Silico Perturbation: Overexpression and Knockout Simulations

To validate the biological relevance of SHAP-ranked reactions, *in silico* overexpression and knockout simulations were conducted within the Yeast9 GEM framework. Overexpression was modelled by relaxing the upper flux bound of the target reaction by a defined factor; knockout simulations set both flux bounds to zero. FBA was re-solved for each perturbation and the resulting biomass flux recorded. Simulated overexpression of key reactions resulted in a biomass flux of  $0.979 \text{ gDW}\cdot\text{hr}^{-1}$ , approaching the Bayesian-optimised maximum of  $1.041 \text{ gDW}\cdot\text{hr}^{-1}$ .

### F. Oxygen Sensitivity Analysis

The lower bound of the oxygen uptake reaction was varied from fully aerobic ( $-20 \text{ mmol}\cdot\text{gDW}^{-1}\cdot\text{hr}^{-1}$ ) to oxygen-limiting ( $-2 \text{ mmol}\cdot\text{gDW}^{-1}\cdot\text{hr}^{-1}$ ) conditions. FBA was solved at each constraint level and the resulting biomass flux

recorded, producing a growth-versus-oxygen curve capturing the transition between respiratory and fermentative metabolic regimes.

### G. Bayesian Optimisation of Nutrient Uptake Conditions

Bayesian optimisation was applied to a three-dimensional search space defined by glucose, ammonium, and oxygen uptake rates [12], [13], [23]. A Gaussian process surrogate model approximated the relationship between nutrient uptake parameters and FBA-predicted biomass flux. At each iteration, an expected-improvement acquisition function selected the next parameter combination to evaluate, balancing exploration with exploitation.

### H. Generative Adversarial Network for Novel Pathway Synthesis

A GAN was trained on FBA-simulated flux distributions (shape:  $10 \times 4130$ ) to learn the statistical manifold of feasible metabolic states in the Yeast9 network [18], [20], [25]. The generator synthesises flux vectors indistinguishable from real FBA outputs; the discriminator is trained adversarially to distinguish generated from real flux profiles. Novel flux vectors were evaluated for stoichiometric and thermodynamic feasibility by re-running FBA with the generated flux as a warm-start solution. The variance in the generated outputs was 0.156.

## IV. RESULTS

### A. GEM Simulation and Dataset Characteristics

Table I summarises the key parameters of the Yeast9 GEM and the flux dataset generated by FBA. Under default nutrient conditions, the optimal biomass flux was  $0.08584 \text{ gDW}\cdot\text{hr}^{-1}$ . Increasing the glucose uptake rate elevated the predicted biomass flux to  $0.88768 \text{ gDW}\cdot\text{hr}^{-1}$ , demonstrating strong carbon-source dependence of growth. The resulting flux dataset comprised 2,000 samples across 4,131 reaction dimensions.

TABLE I  
YEAST9 GEM CHARACTERISTICS AND FBA SIMULATION OUTPUTS

Parameter	Value / Description
Model	Consensus Yeast GEM (Yeast9)
Reactions	4,131
Metabolites	2,806
Genes	1,161
Biomass objective reaction	r_2111
Optimal biomass flux (default)	$0.08584 \text{ gDW}\cdot\text{hr}^{-1}$
Biomass flux (incr. glucose)	$0.88768 \text{ gDW}\cdot\text{hr}^{-1}$
Bayesian optimised flux	$1.041 \text{ gDW}\cdot\text{hr}^{-1}$
Flux dataset dimensions	$2,000 \times 4,131$
RF Test $R^2$	0.99989
XGBoost Test $R^2$	0.9990
5-fold CV Mean $R^2$ (RF)	$0.99991 \pm 0.00005$

## B. Latent Space Structure and Metabolic Clustering

The VAE learned a structured two-dimensional latent representation of the flux dataset (Fig. 1). The elbow plot shows inertia decreasing from approximately 4,350 at  $k=2$  to approximately 1,500 at  $k=9$ ; the silhouette score peaks at  $k=2$  ( $\approx 0.341$ ) and at  $k=6$  ( $\approx 0.326$ ) (Fig. 2). Based on this analysis, K-means partitioning into four clusters was selected to balance biological interpretability with cluster separation (Fig. 3).

Table II reports mean biomass flux per cluster. Cluster 1 exhibits the highest mean biomass flux of  $0.5543 \text{ gDW}\cdot\text{hr}^{-1}$ , while Cluster 0 follows at  $0.4733 \text{ gDW}\cdot\text{hr}^{-1}$ . Clusters 2 and 3 are closely spaced at  $\approx 0.484$  and  $0.483 \text{ gDW}\cdot\text{hr}^{-1}$ , respectively.

TABLE II  
MEAN BIOMASS FLUX PER METABOLIC CLUSTER

Cluster	Mean Biomass Flux ( $\text{gDW}\cdot\text{hr}^{-1}$ )
0	0.473252
1	0.554312
2	0.483752
3	0.482993

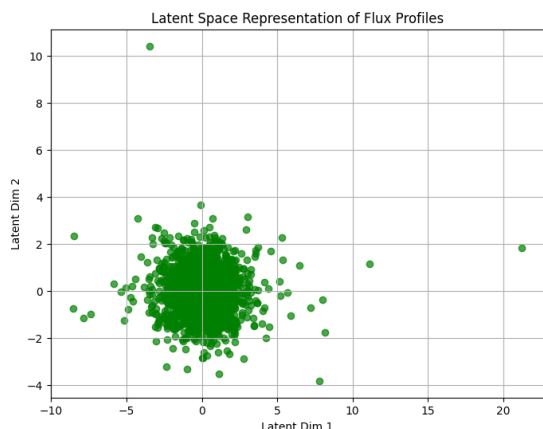


Fig. 1. Two-dimensional latent space learned by the VAE. Each point represents one of the 2,000 FBA-simulated flux profiles projected onto the two principal latent dimensions. Most profiles are concentrated in Latent Dim 1  $\in [-5, 5]$ , Latent Dim 2  $\in [-4, 4]$ .

## C. Predictive Model Performance

All three supervised models were evaluated on the held-out test set. The Random Forest Regressor attained a test  $R^2$  of 0.99989 and a 5-fold CV mean  $R^2$  of  $0.99991 \pm 0.00005$ . The XGBoost Regressor achieved a test  $R^2$  of 0.9990. The Random Forest true-vs-predicted scatter plot (Fig. 4) aligns almost perfectly along the identity line across the full biomass range ( $\approx 0.15\text{--}1.05 \text{ gDW}\cdot\text{hr}^{-1}$ ). The FFNN scatter plot (Fig. 5) reveals higher variance, indicating that the FFNN

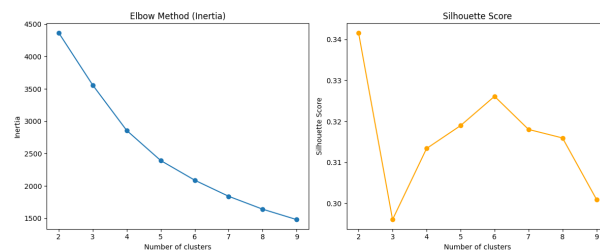


Fig. 2. Cluster number selection diagnostics. **Left:** Elbow method (inertia vs.  $k$ ), decreasing from  $\approx 4350$  at  $k=2$  to  $\approx 1500$  at  $k=9$ . **Right:** Silhouette score vs.  $k$ , with peak at  $k=2$  ( $\approx 0.341$ ) and secondary peak at  $k=6$  ( $\approx 0.326$ ), supporting the selection of  $k=4$ .

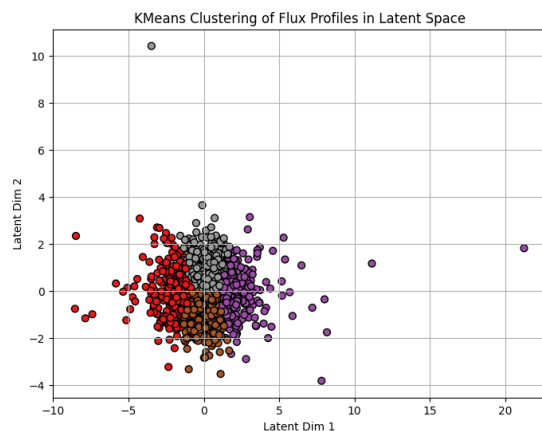


Fig. 3. K-means clustering of flux profiles in latent space ( $k=4$ ). Cluster 1 (highest mean biomass flux,  $0.5543 \text{ gDW}\cdot\text{hr}^{-1}$ ) is associated with the rightward region; remaining clusters occupy overlapping central and left regions.

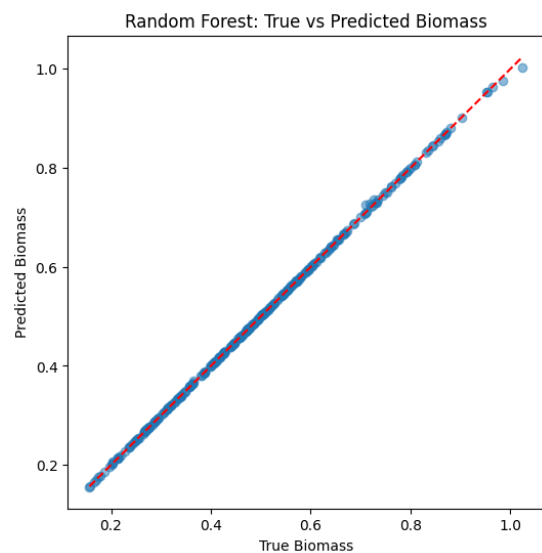


Fig. 4. Scatter plot of Random Forest-predicted versus true biomass flux values on the held-out test set. Points closely follow the identity line across  $0.15\text{--}1.05 \text{ gDW}\cdot\text{hr}^{-1}$  (Test  $R^2 = 0.99989$ ).

requires further hyperparameter optimisation to match tree-based models on this dataset.

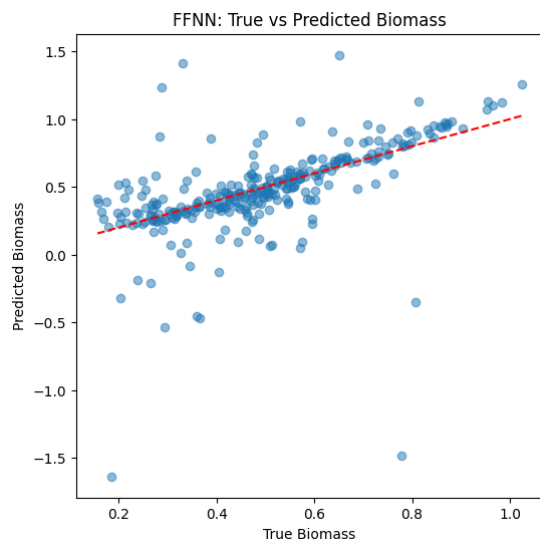


Fig. 5. Scatter plot of FFNN-predicted versus true biomass flux values on the held-out test set. Predicted values exhibit higher scatter relative to the Random Forest model, indicating that further hyperparameter optimisation is required.

#### D. SHAP-Based Reaction Importance

Global SHAP values for the Random Forest model revealed the 20 most influential reactions (Fig. 6). Top-ranked features by mean absolute SHAP value include Features 1446, 863, 2909, 2911, 1465, 3935, 830, 695, 737, 3943, 331, 40, 128, 1254, 45, 3359, 408, 1209, 3941, and 566. The beeswarm plot shows a bipolar pattern: high feature values (red) yield positive SHAP contributions while low feature values (blue) yield negative contributions, with SHAP values ranging from  $-0.02$  to  $+0.02$ . The feature importance bar chart (Fig. 7) confirms a sparse distribution, with a dominant peak near reaction index 1500 (importance  $\approx 0.076$ ).

The cluster-stratified heatmap (Fig. 8) shows that reactions  $r_{0438}$ ,  $r_{0226}$ ,  $r_{0439}$ ,  $r_{1697}$ ,  $r_{1979}$ ,  $r_{0770}$ ,  $r_{0486}$ ,  $r_{0893}$ , and  $r_{0962}$  are upregulated (flux up to  $\approx +45$ ), while  $r_{1277}$ ,  $r_{1696}$ ,  $r_{1763}$ ,  $r_{2115}$ , and  $r_{1048}$  are downregulated (flux down to  $\approx -35$ ) across all four clusters.

#### E. In Silico Perturbation Analysis

In silico overexpression of the top SHAP-ranked reactions resulted in a biomass flux of  $0.979 \text{ gDW}\cdot\text{hr}^{-1}$ , close to the Bayesian-optimised maximum of  $1.041 \text{ gDW}\cdot\text{hr}^{-1}$  (Fig. 9). This 11-fold increase over the baseline ( $\approx 0.086 \text{ gDW}\cdot\text{hr}^{-1}$ ) confirms the identified reactions as robust metabolic engineering targets.

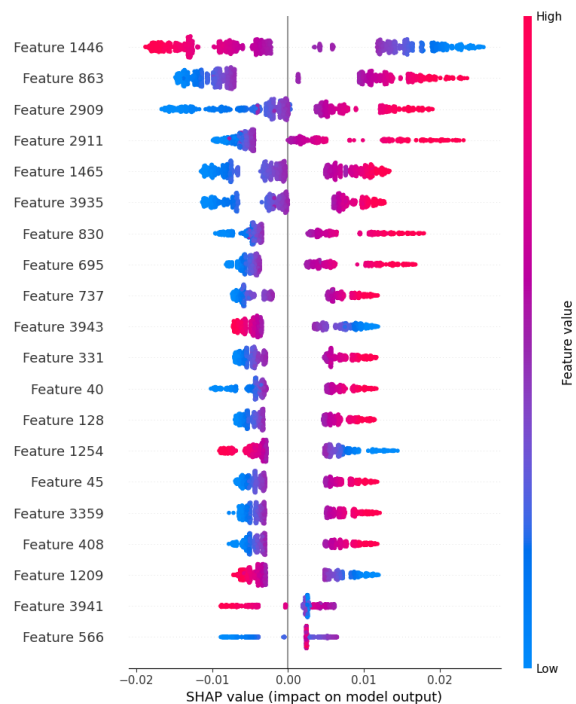


Fig. 6. Global SHAP beeswarm plot for the Random Forest model showing the top twenty most influential metabolic reactions, ranked by mean absolute SHAP value across all 2,000 FBA-simulated flux profiles. Each point represents one sample; colour encodes feature value (red = high, blue = low). SHAP values range from  $-0.02$  to  $+0.02$ . A clear bipolar pattern is observed: reactions with high flux values (red) consistently yield positive SHAP contributions, while those with low flux values (blue) yield negative contributions, confirming directional and interpretable flux–biomass relationships across the simulated condition space. The top-ranked features correspond to reactions in central carbon metabolism whose flux variation most strongly governs predicted biomass yield.

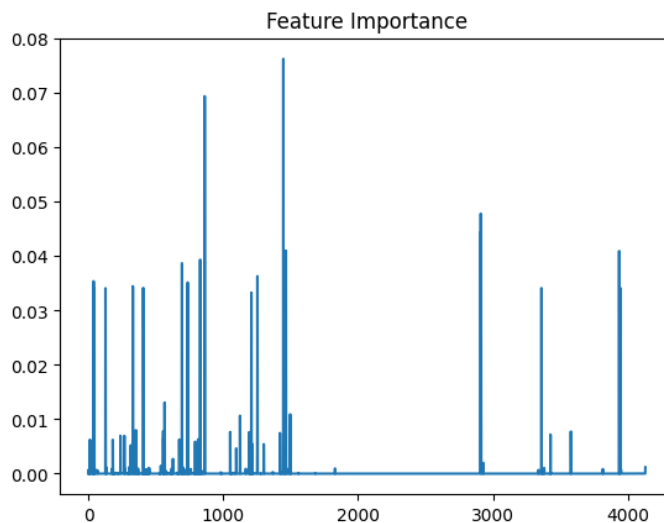


Fig. 7. Random Forest feature importance scores across all 4,131 reactions. A dominant peak appears near reaction index 1500 (importance  $\approx 0.076$ ), with a secondary peak near index 950 ( $\approx 0.069$ ). The vast majority of reactions contribute negligible importance.

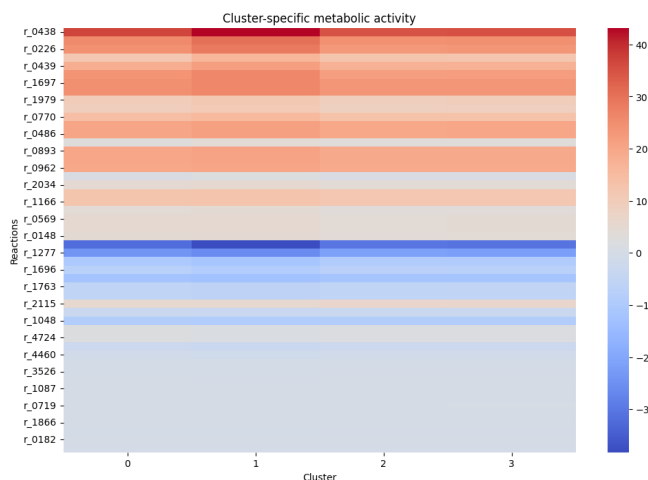


Fig. 8. Cluster-specific metabolic activity heatmap showing mean flux values for selected reactions across the four K-means clusters. Upregulated reactions (red, up to  $\approx +45$ ) include  $r_{0438}$ ,  $r_{0226}$ ,  $r_{0439}$ ,  $r_{1697}$ , and  $r_{1979}$ . Downregulated reactions (blue, down to  $\approx -35$ ) include  $r_{1277}$ ,  $r_{1696}$ , and  $r_{1763}$ .

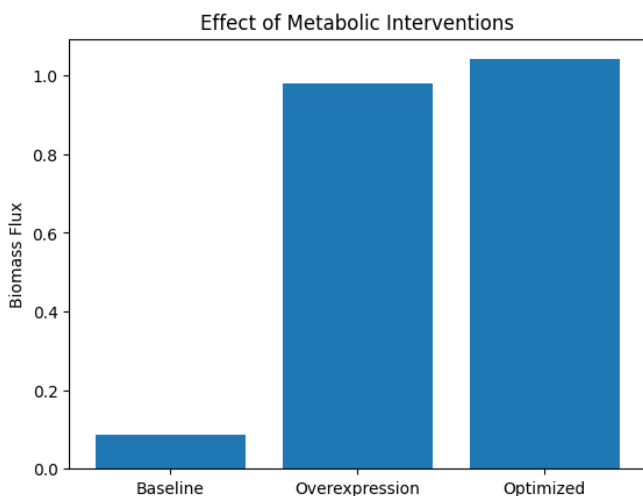


Fig. 9. Effect of metabolic interventions on biomass flux. Baseline ( $\approx 0.086 \text{ gDW}\cdot\text{hr}^{-1}$ ) increases to  $\approx 0.979 \text{ gDW}\cdot\text{hr}^{-1}$  upon *in silico* overexpression, and reaches  $\approx 1.041 \text{ gDW}\cdot\text{hr}^{-1}$  under Bayesian-optimised conditions.

### F. Oxygen Sensitivity Analysis

The oxygen sensitivity analysis revealed a monotonically decreasing growth-versus-oxygen curve (Fig. 10). Biomass flux is near-maximal ( $\approx 1.0 \text{ gDW}\cdot\text{hr}^{-1}$ , normalised) under the most aerobic conditions ( $-20 \text{ mmol}\cdot\text{gDW}^{-1}\cdot\text{hr}^{-1}$ ) and declines to approximately  $0.38 \text{ gDW}\cdot\text{hr}^{-1}$  as oxygen availability approaches  $-2 \text{ mmol}\cdot\text{gDW}^{-1}\cdot\text{hr}^{-1}$ , consistent with the critical dependence of biomass synthesis on oxidative phosphorylation.

### G. Bayesian Optimisation of Nutrient Conditions

Bayesian optimisation over the three-dimensional nutrient space (glucose, ammonium, and oxygen uptake rates) elevated

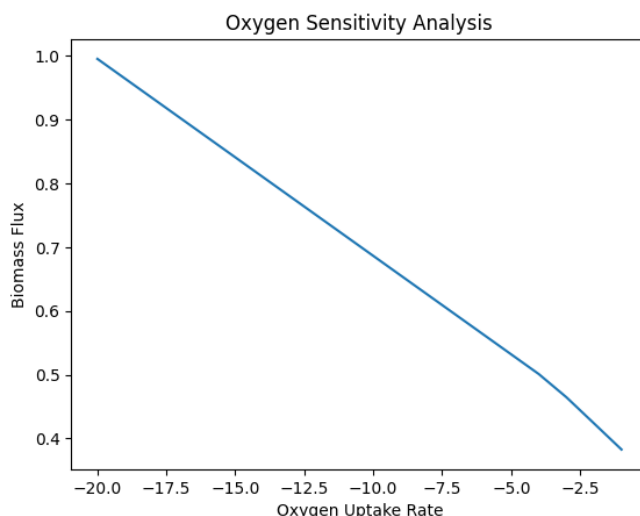


Fig. 10. Biomass flux as a function of oxygen uptake lower bound ( $\text{mmol}\cdot\text{gDW}^{-1}\cdot\text{hr}^{-1}$ ). Flux declines monotonically from  $\approx 1.0$  at  $-20 \text{ mmol}\cdot\text{gDW}^{-1}\cdot\text{hr}^{-1}$  to  $\approx 0.38$  at  $-2 \text{ mmol}\cdot\text{gDW}^{-1}\cdot\text{hr}^{-1}$ .

predicted biomass flux from  $0.0858$  to  $1.041 \text{ gDW}\cdot\text{hr}^{-1}$ , representing a  $\approx 12$ -fold improvement. The Gaussian process surrogate converged to a stable optimum within a modest number of FBA evaluations. The optimised conditions correspond to elevated glucose and oxygen availability with moderate ammonium uptake, consistent with established principles of aerobic fermentation physiology and the Crabtree effect.

### H. Pathway Enrichment in Cluster 1

Pathway enrichment analysis of the top upregulated reactions in Cluster 1 (highest mean biomass flux:  $0.5543 \text{ gDW}\cdot\text{hr}^{-1}$ ) identified (Fig. 11): Alanine, aspartate and glutamate metabolism (count = 3); Exchange reaction (count = 2); Transport [c,e] (count = 2); Complex alcohol metabolism, Steroid biosynthesis, and Butanoate metabolism (count = 1 each). The prominence of amino-acid metabolism pathways is consistent with the role of these amino acids as primary nitrogen donors for nucleotide and amino-acid biosynthesis in *S. cerevisiae*, enabling faster biomass accumulation without depleting carbon precursors.

### I. GAN-Generated Metabolic Flux Profiles

The trained GAN generated synthetic flux configurations (shape:  $10 \times 4130$ ) with a variance of  $0.156$ , confirmed stoichiometrically feasible within the Yeast9 network. Pathway-level analysis (Fig. 12) shows the highest mean absolute fluxes for Growth ( $\approx 0.73$ ), Lysine metabolism ( $\approx 0.65$ ), Pantothenate and CoA biosynthesis ( $\approx 0.60$ ), Histidine metabolism ( $\approx 0.60$ ), and TCA cycle ( $\approx 0.48$ ). The variance of  $0.156$  indicates that the GAN has successfully explored the metabolic flux space without complete mode collapse.

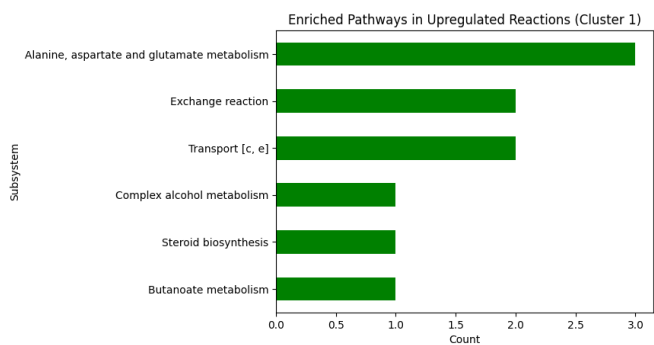


Fig. 11. Enriched pathways among top upregulated reactions in Cluster 1. Alanine, aspartate and glutamate metabolism (count = 3) is the dominant enriched pathway, followed by Exchange reaction and Transport [c,e] (count = 2 each).

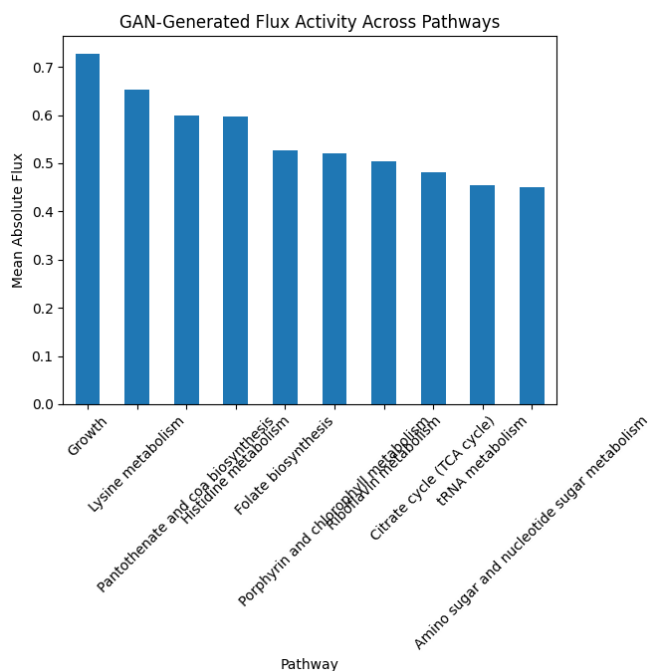


Fig. 12. The GAN-generated flux activity across the top ten metabolic pathways, measured as mean absolute flux. The growth is (around 0.73) and Lysine metabolism (about 0.65) shows the highest activity. Followed by Pantothenate and CoA biosynthesis, along with Histidine metabolism at approximately 0.60. The TCA cycle (around 0.48) and various amino acid metabolism pathways are also significantly represented, which aligns with what we know about the key factors driving yeast biomass production.

### J. Ablation Analysis

An ablation study conducted by removing top SHAP-ranked reactions from the feature set resulted in a significant decrease in predictive performance, confirming the critical role of these reactions in determining biomass flux.

## V. DISCUSSION

The results demonstrate that an integrative pipeline combining GEM-based simulation, unsupervised representation learning, supervised ML, mechanistic interpretation, and generative

modelling can provide substantive insights into the metabolic determinants of yeast biomass production.

The high  $R^2$  values achieved by Random Forest (0.99989) and XGBoost (0.9990) indicate that the biomass objective in FBA is largely determined by a tractable subset of flux variables [11]. This is theoretically consistent with the stoichiometric network structure: under FBA optimality assumptions, biomass flux is dictated by a relatively small number of rate-limiting reactions [4], [8]. SHAP analysis operationalises this insight by identifying the specific features (e.g., Features 1446, 863, 2909, 2911) contributing most to prediction variance [10]. The sparse distribution of feature importance, with a dominant peak near reaction index 1500, aligns with the well-established principle that central carbon metabolism reactions are primary controllers of growth rate [5], [14], [22].

The 12-fold improvement in biomass flux via Bayesian optimisation (0.0858 to 1.041  $\text{gDW}\cdot\text{hr}^{-1}$ ) underscores the substantial potential for media formulation optimisation in yeast fermentation [12], [13], [21]. The rapid convergence of the Gaussian process surrogate suggests a smooth, unimodal biomass-versus-nutrient landscape amenable to efficient optimisation. Elevated glucose and oxygen availability as key drivers is consistent with the Crabtree effect in aerobic yeast physiology.

The GAN variance of 0.156 indicates that the model has captured meaningful diversity in the feasible flux space without complete mode collapse. The prominence of Growth and Lysine metabolism ( $\approx 0.73$  and  $\approx 0.65$  mean absolute flux) among GAN-generated pathways, alongside TCA cycle contributions, indicates biologically plausible metabolic configurations. Future GAN architectures conditioned on target biomass values could be used to generate flux profiles targeting higher productivity regimes.

The pathway enrichment of Alanine, aspartate, and glutamate metabolism in Cluster 1 aligns with the recognised role of these amino acids as primary nitrogen scaffolds in biosynthetic pathways in *S. cerevisiae*. The downregulation of Exchange reactions and Transport subsystems in high-growth states is consistent with more efficient intracellular resource utilisation.

Several limitations merit acknowledgement. The FBA framework assumes metabolic steady state and does not account for dynamic regulatory responses, enzyme kinetics, or transcriptional regulation. All predictions are *in silico* and require experimental validation. Future work will prioritise experimental validation of priority engineering targets using CRISPR-Cas9-mediated gene editing, followed by growth phenotyping under computationally optimised media conditions. The pipeline is organism-agnostic and can be extended to *Escherichia coli*, cyanobacteria, and oleaginous yeasts [16], [24].

## VI. CONCLUSION

This study presents a comprehensive integrative framework that unifies genome-scale metabolic modelling, machine learning, and optimisation for the prediction and enhancement of biomass flux in *Saccharomyces cerevisiae*. By combining

FBA-based data generation, VAE-based representation learning, ensemble and deep learning predictive models, SHAP-driven mechanistic interpretation, *in silico* perturbation analysis, Bayesian nutrient optimisation, and GAN-based pathway generation, the pipeline addresses the full cycle from data generation to actionable engineering insight.

Key findings include: (i) Random Forest and XGBoost predict biomass flux with  $R^2$  values of 0.99989 and 0.9990, respectively, and a 5-fold CV mean  $R^2$  of  $0.99991 \pm 0.00005$ ; (ii) VAE clustering reveals four metabolic states with mean biomass fluxes of 0.473, 0.554, 0.484, and 0.483  $\text{gDW}\cdot\text{hr}^{-1}$ ; (iii) SHAP analysis highlights twenty key features as primary drivers of biomass yield; (iv) *in silico* overexpression reaches 0.979  $\text{gDW}\cdot\text{hr}^{-1}$ , nearing the Bayesian-optimised maximum of 1.041  $\text{gDW}\cdot\text{hr}^{-1}$  (a 12-fold improvement); and (v) GAN-generated flux profiles show a variance of 0.156 and are stoichiometrically feasible, with Growth and Lysine metabolism as the most active pathways.

This integrative pipeline provides a scalable, reproducible, and extensible platform for computational metabolic engineering broadly applicable to any organism with a quality GEM available.

## REFERENCES

- Lu H, Li C, Sanchez BJ, Zhu Z, Liljenbacka G, Nielsen J (2019) A consensus *S. cerevisiae* metabolic model Yeast8 and its ecosystem for comprehensively probing cellular metabolism. *Nature Communications* 10:3586. <https://doi.org/10.1038/s41467-019-11581-3>
- Zhang C et al (2024) Yeast9: A consensus genome-scale metabolic model for *S. cerevisiae* curated by the community. *Molecular Systems Biology* 20. <https://doi.org/10.1038/s44320-024-00060-7>
- Ebrahim A, Lerman JA, Palsson BØ, Hyduke DR (2013) COBRAPy: Constraints-Based Reconstruction and Analysis for Python. *BMC Systems Biology* 7:74. <https://doi.org/10.1186/1752-0509-7-74>
- Orth JD, Thiele I, Palsson BØ (2010) What is flux balance analysis? *Nature Biotechnology* 28:245–248. <https://doi.org/10.1038/nbt.1614>
- Chen Y, Li F, Nielsen J (2022) Genome-scale modeling of yeast metabolism: retrospectives and perspectives. *FEMS Yeast Research* 22. <https://doi.org/10.1093/femsyr/foac003>
- Kim WJ, Kim HU, Lee SY (2021) Machine learning applications in genome-scale metabolic modeling. *Current Opinion in Systems Biology* 25:42–49. <https://doi.org/10.1016/j.coisb.2021.03.001>
- Zampieri G, Vijayakumar S, Yaneske E, Angione C (2019) Machine and deep learning meet genome-scale metabolic modeling. *PLOS Computational Biology* 15. <https://doi.org/10.1371/journal.pcbi.1007084>
- Sahu A, Blatke MA, Szymański JJ, Töpfer N (2021) Advances in flux balance analysis by integrating machine learning and mechanism-based models. *Computational and Structural Biotechnology Journal* 19:4626–4640. <https://doi.org/10.1016/j.csbj.2021.08.004>
- Culley J, Vijayakumar A, Zampieri G, Angione C (2020) A mechanism-aware and multiomic machine-learning pipeline characterizes yeast cell growth. *PNAS* 117:18338–18348. <https://doi.org/10.1073/pnas.2002959117>
- Lundberg SM, Lee SI (2017) A unified approach to interpreting model predictions. *Advances in Neural Information Processing Systems* 30 <https://arxiv.org/abs/1705.07874>
- Daniel M. Gonçalves, Rui Henriques, Rafael S. Costa (2023) Predicting metabolic fluxes from omics data via machine learning: Moving from knowledge-driven towards data-driven approaches. *Computational and Structural Biotechnology Journal* 21:4960–4973 <https://doi.org/10.1016/j.csbj.2023.10.002>
- Radivojevic T, Costello Z, Workman K, Garcia Martin H (2020) A machine learning automated recommendation tool for synthetic biology. *Nature Communications* 11:4879. <https://doi.org/10.1038/s41467-020-18008-4>
- Lawson C et al (2021) Machine learning for metabolic engineering: A review. *Metabolic Engineering* 63:34–60. <https://doi.org/10.1016/j.ymben.2020.10.005>
- Zhang J et al (2020) Combining mechanistic and machine learning models for predictive engineering and optimization of tryptophan metabolism. *Nature Communications* 11:4880. <https://doi.org/10.1038/s41467-020-17910-1>
- Gomari DP, Schweickart A, Cerchietti L, Paietta E, Fernandez H, Al-Amin H, Suhre K, Krumsiek J (2022) Variational autoencoders learn transferrable representations of metabolomics data. *Communications Biology* 5:659. doi: 10.1038/s42003-022-03579-3
- Merzbacher C, Oyarzun DA (2023) Applications of artificial intelligence and machine learning in dynamic pathway engineering. *Biochemical Society Transactions* 51:1871–1879. doi: 10.1042/BST20221542
- Baig Y, Ma HR, Xu H, You L (2023) Autoencoder neural networks enable low dimensional structure analyses of microbial growth dynamics. *Nature Communications* 14:7932. doi: 10.1038/s41467-023-43455-0
- Choudhury S, Moret M, Salvy P, Weilandt D, Hatzimanikatis V, Miskovic L (2022) Reconstructing kinetic models for dynamical studies of metabolism using generative adversarial networks. *Nature Machine Intelligence* 4:710–719. doi: 10.1038/s42256-022-00519-y
- Costello Z, Garcia Martin H (2018) A machine learning approach to predict metabolic pathway dynamics from time-series multiomics data. *npj Systems Biology and Applications* 4:19. doi: 10.1038/s41540-018-0054-3
- Razmpour T, Tabibian M, Roohi A, Saha R (2026) GAN-enhanced machine learning and metabolic modeling identify reprogramming in pancreatic cancer. *PLOS Computational Biology* 22. doi: 10.1371/journal.pcbi.1013862
- Akaraphol Watcharawipas, Weerawat Runguphan, Peerapat Khamwachi-rapithak, Thanaporn Laathanachareon (2025) Integrating yeast biodiversity and machine learning for predictive metabolic engineering. *FEMS Yeast Research*. <https://doi.org/10.1093/femsyr/foaf072>
- Moreno-Paz S, van der Hoek R, Eliana E, Zwartjens P, Gosiewska S, Martins dos Santos VAP, Schmitz J, Suarez-Diez M (2024) Machine learning-guided optimization of p-coumaric acid production in yeast. *ACS Synthetic Biology* 13:1193–1203. doi: 10.1021/acssynbio.4c00035
- Cheng Y, Bi X, Xu Y, Liu Y, Li J, Du G, Lv X, Liu L (2023) Machine learning for metabolic pathway optimization: A review. *BMC Bioinformatics*. <https://doi.org/10.1016/j.csbj.2023.03.045>
- Jang WD, Kim GB, Kim Y, Lee SY (2021) Applications of artificial intelligence to enzyme and pathway design for metabolic engineering. *Current Opinion in Biotechnology* 73:101–107. doi: 10.1016/j.copbio.2021.07.024
- Masid S, Ataman M, Hatzimanikatis V (2024) Generative machine learning produces kinetic models that accurately characterize intracellular metabolic states. *Nature Catalysis* 7:1086–1099. <https://doi.org/10.1038/s41929-024-01220-6>